Absolute emission cross sections for electron-impact excitation of the $3p$-$3s$ transition in Al^{2+}

G. H. Dunn,[1] D. S. Belić,[2] C. Cisneros,[3] D. H. Crandall,[4] R. A. Falke,[5]
and D. Gregory[6]
[1]*JILA, University of Colorado, and NIST, Boulder, Colorado 80309-0440*
[2]*Faculty of Physics, Belgrade University, Belgrade, Yugoslavia*
[3]*Centro de Ciencias Físicas, UNAM. Cuernavaca, Mor., Mexico*
[4]*NA-11, 4C012 FOR, US DOE, Washington DC 20545*
[5]*Optometrix Inc., Seattle, Washington 98058*
[6]*Oak Ridge National Laboratory, P.O. Box 2008, Oak Ridge, Tennessee 37831-6375*

(Received 19 April 2002; published 18 September 2002)

Crossed beams of electrons and Al^{2+} ions combined with fluorescence detection were used to measure the absolute cross section for electron-impact excitation of the ions to yield 186.3 nm and 185.5 nm photons from the $3s$-$3p$ transition. The measured cross section near the 6.7 eV threshold energy is about 16×10^{-16} cm^2, and some resonance structure near threshold is indicated. Total relative uncertainties (1σ) are typically about 6%, to be combined with an 11% absolute calibration uncertainty. Total uncertainties at high confidence level (90%) are around 20%, using a coverage factor of 1.7. Comparisons made with various theoretical calculations, specifically distorted wave and nine-state close coupling, show better agreement of experimental values with distorted wave calculations, with the measured values being higher near threshold than the most recent close-coupling calculations.

DOI: 10.1103/PhysRevA.66.032706 PACS number(s): 34.80.Kw

I. INTRODUCTION

Calculation and measurement of cross sections for electron-impact excitation of ions has been an active area of research for several decades, heavily motivated by the important role played by these processes in various hot plasma environments—most notably astrophysical, controlled fusion, and atmospheric explosions. Calculations have matured to the point that scientists in large international consortia [1] calculate and make available many thousands of cross sections. This is not to say that theoretical results have been experimentally tested to the point that one can have unflinching faith in them. Indeed, it has been shown in a number of cases—especially where resonances play a major role—that painstaking care is required, since a small error in calculating resonance positions can lead to mistakes in the amount of interference, and thence to incorrect cross sections.

Aluminum is influential in a number of plasma and astrophysical environments. For one example, Al^{2+} emission lines have been observed in the solar ultraviolet spectrum with the ratio of their line intensities considered as useful temperature diagnostics [2]. Because of the importance, a number of calculations [3–7] of excitation rates and cross sections have been performed. In this paper we will make specific comparisons with the distorted-wave calculations of Merts *et al.* [6] and the close-coupling calculations of Mitroy and Norcross [8].

Experimental efforts to test theory for electron-impact excitation of ions at first focused on plasma rate measurements [9]. Later, crossed beams of electrons and ions with fluorescence detection were employed [10], and this technique has accounted for a major share of the data and experimental tests of theory. Because of experimental limitations most of the data obtained using this method have involved singly charged ions with only a few cases of measurements on multiply charged ions. In recent years, a merged electron-ion-beams electron-energy-loss technique has been introduced [11,12]. Because of superior energy resolution compared to the other methods, it has produced some of the best data for exploring the role of resonances in excitation cross sections, and because of larger interaction volumes and superior signal detection efficiency it has allowed making measurements on more highly charged ions and a broader variety of species. This newer method is, however, confined to measurements relatively close to threshold. Still another relatively recent innovation for study of multiply charged ions (particularly effective for very highly charged ions) is the use of the electron-beam ion trap [13] and related source/trap methods. There are other methods that account for a smaller fraction of electron-ion excitation investigations. The various techniques and results have been reviewed [14] a number of times over the years.

Here we report one of the very few measurements on *multiply charged* ions using the crossed-beams–fluorescence detection method. Cross sections for multiply charged ions using this technique have been published [15–18] on C^{3+}, N^{4+}, and Hg^{2+}. This work on Al^{2+} has been briefly reported [19] in abstract form previously, but we neglected proper publication of the results. Since results on the same excitation using the merged-electron-ion beams energy loss (MEIBEL) technique have recently been obtained [20], it was deemed important to make a comprehensive report of this work and results so that a proper comparison could be made.

The process under investigation here is for the sodiumlike ion, Al^{2+},

$$Al^{2+}(3s\ ^2S)+e\rightarrow Al^{2+}(3p\ ^2P^o)+e\rightarrow Al^{2+}(3s\ ^2S)+e+h\nu, \tag{1}$$

 ©2002 The American Physical Society

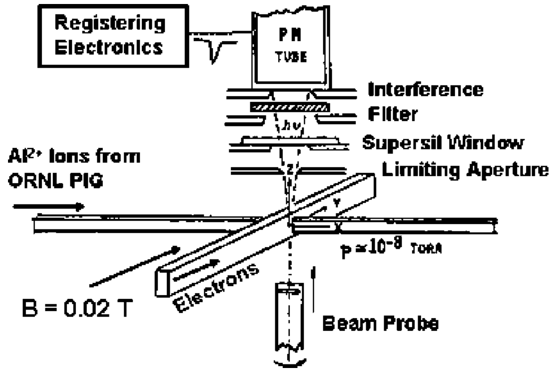

FIG. 1. Schematic illustration of the experimental apparatus.

where the photon wavelength is 186 nm and the threshold interaction energy is 6.6 eV. At as low an energy as 14.3 eV, one may excite the $3d\ ^2D$ level, which can cascade through the $3p\ ^2P^o$ state and thus, provided the resultant photon reaches the detector, this excitation will also be detected. That is to say, excitation of higher levels followed by cascade through the $3p\ ^2P^o$ state, giving rise to 186 nm radiation that reaches the detector will be part of the measurement. Hence, the measurement here is that of an *emission* cross section rather than an *excitation* cross section except below 14.3 eV, where only the $3p\ ^2P^o$ level is energetically accessible. Labeling the ground state, $3s\ ^2S$, with g; the detected emitting state, $3p\ ^2P^o$, with f; and the cascading states with the running index, j; we thus have, for the measured emission cross section, σ_{em}, in terms of the respective excitation cross sections, σ_{ex},

$$\sigma_{em}(f\rightarrow g)=\sigma_{ex}(g\rightarrow f)+\sum_{j>f}\gamma(j\rightarrow f)\sigma_{ex}(g\rightarrow j), \quad (2)$$

where $\gamma(j\rightarrow f)$ is the branching fraction from j to f. The doublet nature of the system is not taken into account here, as the $^2P_{1/2}$ and $2P_{3/2}$ levels are separated by only 29 meV, and the emission lines of 185.47 and 186.28 nm are not separable in the spectroradiometer used here.

Experimental *excitation* cross sections near threshold measured using the MEIBEL technique have been reported previously for other Na-like ions: Mg^+ [21], Si^{3+} [22], Cl^{6+} [23], and Ar^{7+} [24]. Generally, good agreement has been found between the experimental values and those calculated using close-coupling theoretical methods.

II. EXPERIMENTAL APPROACH

A. General

The experiment was performed using the crossed-beams apparatus at Oak Ridge National Laboratory. Thus, the technique is closely allied to that reported previously for measurements [15,16] on C^{3+} and N^{4+}, and many details of the method can also be found in Refs. [25,26] on excitation of singly charged ions. A schematic illustration of the experimental configuration is shown in Fig. 1. Ions from the source (ORNL PIG) [27] are extracted and accelerated by a 10 kV potential and are then mass-to-charge analyzed. They are guided to the collision region via an assortment of electrostatic lenses where they are traveling in the x direction and a magnetically (0.02 T) confined, variable-energy beam of electrons traveling in the y direction collides with them. Photons emitted by the excited ions into a fixed and known solid angle centered about the z direction pass through a defining aperture, a supersil window, and an interference filter, and their numbers are measured by counting them using a calibrated vacuum ultraviolet photomultiplier. A scanning slit beam probe is used to measure the ion and electron distributions in the z dimension for the two beams. Beam particles are collected in appropriate Faraday cups and their currents are measured.

Both beams impact background gas and some surfaces, producing photons that are detected by the photomultiplier. To separate the photons produced from the beam-beam interaction from these background events, both beams were chopped and two registering scalers were gated in a manner [28] that the difference in events recorded by the scalers is the desired signal. Signal counts using this scheme are collected over only about one quarter of the time, with background from the electrons, background from the ions, and dark background being collected during the other three quarters, respectively. The emission cross section is calculated from the measured quantities using the expression [29]

$$\sigma=\frac{1}{Y_\Omega}\frac{R}{I_eI_i}\frac{qe^2\nu_i\nu_e}{(\nu_i^2+\nu_e^2)^{1/2}}\frac{F}{D(z_0,\lambda)}, \quad (3)$$

where R is the photon signal count rate, qe is the charge of the ion, e is the electron charge, I_i and I_e are the total currents of ions and electrons, respectively, and v_i and v_e are their respective laboratory velocities. The factor F, with units of length, accounts for the spatial overlap of the ion and electron beams with spatial distributions $R(z)$ and $G(z)$, respectively, and it includes the relative spatial variation of the detection sensitivity $\eta(z,\lambda)$. It can be represented by

$$F=\int R(z)dz\int G(z)dz\bigg/\int R(z)G(z)\eta(z,\lambda)dz, \quad (4)$$

where

$$\eta(z,\lambda)=D_R(z,\lambda)-I_1+(e^{w_e/\nu_i\tau}-1)I_2 \quad (5)$$

with

$$I_1=\int_0^{w_e}e^{-x/\nu_i\tau}D_R(x,z,\lambda)dx\bigg/\int_0^{w_e}D_R(x,z_0,\lambda)dx \quad (6)$$

and

$$I_2=\int_{w_e}^{\infty}e^{-x/\nu_i\tau}D_R(x,z,\lambda)dx\bigg/\int_0^{w_e}D_R(x,z_0,\lambda)dx. \quad (7)$$

The average probability that a photon of wavelength λ emitted in an arbitrary direction from the $z=z_0$ plane in the collision volume will be counted is given by $D(z_0,\lambda)$. The quantity $D_R(z,\lambda)$ is the relative variation of that probability with height z such that $D_R(z_0,\lambda)=1$. $D_R(x,z,\lambda)$ is the relative probability averaged over the width of the ion beam that a photon emitted from a line parallel to the electron beam will be detected, w_e is the width of the electron beam, and τ is the lifetime associated with the transition giving photons of wavelength λ. The subtraction of I_1 in Eq. (5) is to account for the fact that some ions, due to the finite lifetime of the excited state, do not radiate while within the electron beam, and the term with I_2 accounts for emission beyond the electron beam which is still detected. In this experiment the integrations over x can be ignored, since the beam travels at v_i 3.8×10^7 cm/s, and $\tau\approx2$ ns. The quantity Y_Ω corrects for anisotropy in the radiation, and is given by

$$Y_\Omega=(1-P\langle\cos^2\theta\rangle_\Omega)\Bigg/\left(1-\frac{1}{3}P\right), \tag{8}$$

where the $\cos^2\theta$ term is averaged over the solid angle Ω subtended by the detector at the point of emission. In this experiment the polarization P is not measured, but it is estimated to be small based on theoretical considerations as discussed later. Hence, Y_Ω is near unity.

B. Ion beam

The Al^{2+} ions were formed by situating a rod of aluminum directly into the ORNL PIG [27] and using CCl_4 as the discharge gas. Free chlorine in the Penning discharge in contact with the hot aluminum makes aluminum chloride, which has a high enough vapor pressure to yield a significant amount in the vapor phase. The discharge was located between the poles of a large magnet (previously a cyclotron magnet), and a pair of curved plates near the exit hole of the source produces an electrostatic field transverse to the magnetic field, so that ions of a particular mass-to-charge ratio are directed through an exit aperture placed outside the magnetic field in a sort of Wien filter arrangement. The ion source was held at +10 kV, so that in grounded transport regions and at the interaction region, the Al^{2+} ions had an energy of 20 keV and a velocity of 3.8×10^7 cm s^{-1}. In the interaction region the confining magnetic field for the electrons causes deflection of the ions, and this is offset by parallel plate deflectors before and after the entrance to the electron gun. Typical ion currents at the collision region during the experiment were of order 1 μA. The height of the ion beam was of order 3 mm, and the ion beam "fit within" the electron beam. Calibrated current integrators of the charge-to-frequency conversion type were used to measure the ion current collected in the Faraday cup which had a suppressor electrode to prevent escape of secondary electrons.

C. Electron beam

The electron beam is from a gun [30] adapted from a design that was carefully studied and reported [25,31]. The gun is immersed in a magnetic field (0.02 T) generated by permanent magnet rods between pole faces. This allows the attainment of a moderately high density beam even at low electron energies. The electrons were accelerated from a hot cathode by a series of slotted plates maintaining a uniform electric field parallel to the magnetic field, thus minimizing spiraling of the electrons along the path. The beam was chopped by applying a square pulse more negative than the cathode to one of the electrodes. Typical electron currents ranged from 10 μA to 320 μA between 10 and 100 eV and were measured with a calibrated current to frequency convertor. The beam was approximately 5 mm high and less than 2 mm wide.

The electron collector was strongly biased. This serves two purposes, the first of which is to prevent secondary electrons from escaping. Second, a problem with magnetically confined electron beams is that it is difficult to ensure that there are no electrons elastically reflected from the collector entering the beam and traveling in the "opposite" direction. The strong bias and closely spaced razor blades on the collector helped to minimize this, i.e., only in a very small angular cone (growing smaller with bias) could elastically reflected electrons overcome the potential barrier presented by the bias. At higher electron energies, however, the bias was typically too weak to totally ensure nonreflection of beam. Hence, one-sided uncertainties attendant to this must be assessed at the highest electron energies.

The electric field from the ion beam deflectors which compensated for the magnetic field of the electron gun leaked into the gun region and compromised the electron energy distribution. Typically, this gun design [25,31] has exhibited an electron energy distribution of about 0.4 eV full width at half maximum (FWHM). However, with the degrading fields just mentioned, the energy distribution ΔE is here broadened to about 1.5 eV FWHM as determined by the rise with energy from threshold of the excitation cross section measured here with this modified gun. Normally, if there are no resonances at threshold, electron-ion excitation cross sections rise with infinite slope at threshold (step function) [32]. Thus, the derivative of the experimental curve at threshold gives the energy distribution.

D. Photon detection and radiometry

The spectroradiometer illustrated in Fig. 1 consists of a defining aperture in the collision box, a supersil vacuum window, an interference filter [33], and a photomultiplier (PMT) [34] with appropriate electronics. The distance from the beam line was carefully measured, as were all apertures and the transmission of the window. The filter transmission was carefully measured as a function of angle and that information was incorporated into the data analysis. The effect of the increased path length due to the vacuum window was taken into account. The cell between the window and the photomultiplier was filled with argon, and tests were made to ensure that there was no absorption of photons in this cell by that gas.

An absolute calibration of the system was made and tests performed as described in the Appendix. A detailed evaluation of $D_R(z,\lambda)$ was made by mapping the response of the photomultiplier over its surface. The absolute sensitivity $D(z_0,\lambda)$ was determined to be 4.98×10^{-5} counts per photon.

E. The anisotropy factor

The anisotropy factor, Y_{Ω}, shown in Eq. (8) involves knowledge of the polarization P of the emitted radiation and the solid angle Ω. Percival and Seaton [35] have shown that for ${}^2P \rightarrow {}^2S$ multiplets, an initial polarization of 0.43 is expected at threshold, going to -0.27 at high energy (ignoring cascade) for electron impact excitation of *neutral atoms* and detection perpendicular to the electron beam. For excitation of *ions* it is expected that the threshold polarization will be reduced due to the Coulomb field mixing of higher partial waves. Previous measurements [25] and theory [36] suggest that this threshold reduction factor is probably about 1/3. For sodium-like ions it is expected that the fine and hyperfine couplings (for ^{27}Al, $I=5/2$) will cause any initial polarization of the orbital angular momentum, which gives rise to polarized photons, to be converted into polarization of electron and nuclear spins. The formalism of Fano and Macek [37] can be used to calculate this effect when the lifetime of the state and fine and hyperfine splittings are known. Calculation for ${}^{27}Al^{2+}$ gives a photon polarization reduction by 0.13, leading to an expected polarization of 0.018 at threshold going to -0.035 at high energy. The attendant anisotropy factor is then expected to differ from unity by the order 1% at all energies. Due to the approximate nature of the estimates, the small correction is not applied to the data, and a one-sided energy-dependent uncertainty is assessed.

F. Experimental tests

Colliding charged particle beams are notorious [38] for spurious signals when the backgrounds from both beams are high compared to the true signal. Thus, the space charge of one beam can slightly alter the trajectories (and in turn the background caused by the beam) of the other beam leading to unwanted signatures of beam-beam interactions appearing in the detector. Various tests help to ensure that these effects are not significant for the cross sections measured. In this context, the beam currents, the ambient pressure, and the chopping frequency were varied in experimental tests, and no systematic effects were found in the data. The absence of apparent signal below the energetic threshold is also taken as evidence that space charge effects did not influence the data reported here.

III. RESULTS AND DISCUSSION

The measured cross sections are shown for 25 interaction energies in Fig. 2. The hollow square points are shown with *relative* uncertainties at the 1σ level. At six energies, shaded circular points are superimposed on the relative points and these six points are shown with total *absolute* uncertainties U with a coverage factor of 1.7 so that the confidence level is 90%. There is the impression that a resonance structure appears near 12 eV, about 2 eV below the onset of cascade. As noted earlier, the rise of the cross section from threshold defines the experimental electron energy spread, since with zero energy spread one expects an infinite slope at threshold. A Gaussian distribution of 1.5 eV FWHM fits the rise satisfactorily.

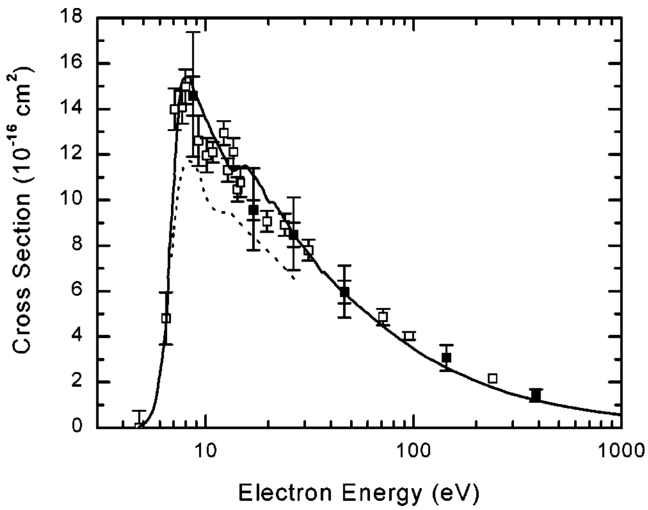

FIG. 2. Experimental cross sections vs interaction energy. Hollow square points are shown with relative uncertainties at the 1σ level; shaded circular points at six energies are superimposed on the square ones and are shown with total expanded uncertainties U with a coverage factor of 1.7 believed to be at about the 90% confidence level. Upper solid curve represents UDW calculations of Merts *et al.* [6] including some cascade as discussed in the text. Lower solid curve is from a CCV9 calculation of Mitroy and Norcross [8]. Both theoretical curves have been convoluted with a 1.5 eV FWHM Gaussian energy distribution.

Sources of uncertainty are listed in Table I. In the assessment of uncertainties, two-sided symmetric uncertainties have been combined in quadrature, and one-sided uncertainties have been linearly added to the result.

TABLE I. Individual sources of total uncertainty U in the cross section measurement; presented with a coverage factor of 1.7 in an attempt to make them equivalent to 90% confidence level.

Sources of uncertainty in emission cross section determination	U at "high" (90%) C.L. in %
Spectroradiometry, exclusive of one-sided anisotropy uncertainty	± 16.7
Electron current measurement	± 1.7
Ion current measurement	± 1.7
Beam overlap factor	± 3
Photon counting efficiency	± 3
Ion velocity	± 0.5
Uncollected beam currents	± 1
"Typical" statistical uncertainty in data	± 10
Quadrature sum of two-sided uncertainties	± 20
One-sided uncertainty, anisotropy:	
Low E	$+0.9$
High E	-2
One-sided uncertainty, reflected electrons:	
Low E	-0
High E	-2
Total U at "high" (90%) C.L.:	
Low E	$+21, -19$
High E	$+16, -24$

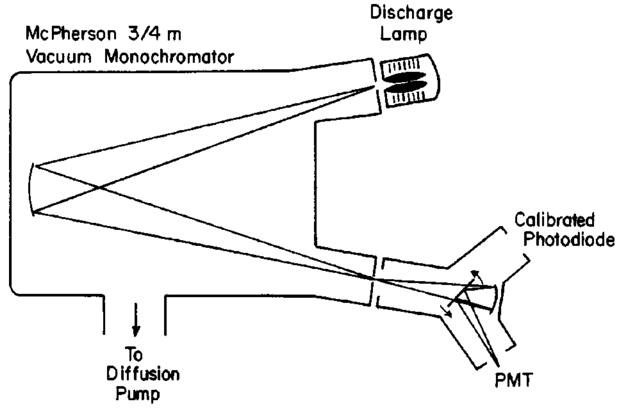

FIG. 3. Schematic arrangement for calibrating the PMT detector [34] against a NIST precalibrated photodiode [39].

Figure 2 also shows results of the convolution of the 1.5 eV FWHM Gaussian energy distribution with the data from two different theoretical calculations. The top curve in the figure represents the unitarized distorted waves (UDW) cross sections from Merts *et al.* [6]. The plotted curve contains results calculated from Eq. (2), where the final radiating state, $3p\ ^2P$, and cascade to that state from the $3d$, $4s$, $4d$, $4f$, and $5s$ levels have been included. The lifetime associated with cascade from the $3d$ and $4s$ levels to the $3p$ level is around 0.7 ns, so the associated $3p$-$3s$ photons readily reach the detector. The theory indicates that these two cascades account for about 90% of the cascade radiation, and that cascade contributes about 10% to the total signal; thus detailed lifetime and branching analysis was not carried out for cascade from the other levels. Taken in the absence of other considerations, the agreement between the experiment and the UDW results is good.

Also shown in the figure as the lower curve is the convoluted result of a nine-state close-coupling calculation of Mitroy and Norcross [8]. These authors carried out an extensive investigation of the process under study including four different theoretical approximations. The most complete is that shown, and it includes close coupling of the $3s$, $3p$, $3d$, $4s$, and $4p$ levels with $4d$, $4f$, $5s$, and $5p$ pseudostates coupled in as well. Two-body polarization potentials were included in the scattering Hamiltonian, and semiempirical (giving ''best'' eigenenergies) Hartree-Fock wave functions were employed. This CCV9 calculation agreed well with the similar CCV5 (without pseudostates) results and less well with a five-state close-coupling calculation not including polarization potentials, a calculation with results lying intermediate to the CCV9 and UDW results. The CCV9 results [8] show a sharp drop in the cross section for excitation to the $3p$ level at an energy very close to where cascade sets in. The cascade contribution from the $3d$, $4s$, and $4p$ levels adds to the total emission cross section in a way that a rather smooth curve is predicted in this region of energy. However, resonances can clearly be seen in the nonconvoluted CCV9 results [8] at energies below the cascade onset. Such resonances are extremely sensitive to details of the calculations, and the apparent feature at 12 eV in the experiment may well be related to those calculated.

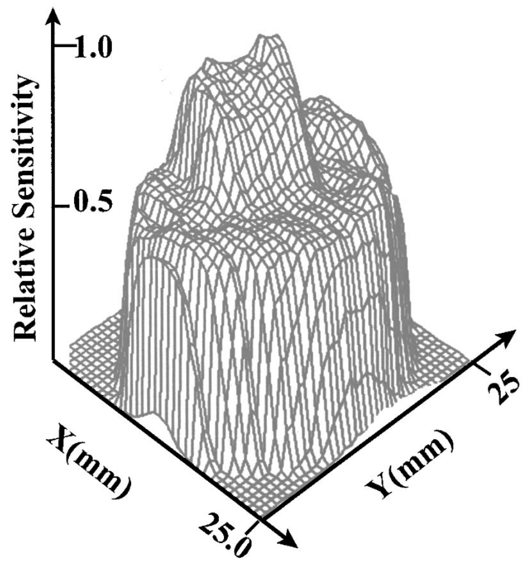

FIG. 4. Variation of PMT [28] sensitivity over its surface.

Clearly, the experimental results cannot be said to agree well in magnitude with what one regards as the most sophisticated and complete theoretical data. Unfortunately, however, the present experiment does not separate the theoretical results in a definitive way. The experimental values are seen to lie just at or within the total expanded uncertainties at 90% confidence level, meaning that if one were to perform the same experiment over again including new calibrations and measurements, the chances are about 10% that there would be ''good'' agreement with the more sophisticated theory. The dominant uncertainty in the experiment is the radiometric calibration, and, as seen in the Appendix, the largest contribution there comes from the calibration by NBS (now NIST) of the diodes used for transfer to the photomultiplier detector in the experiment.

As the results stand, the UDW results are favored over those of the CCV9 method. However, as mentioned earlier, a recent experiment [20] using the MEIBEL technique that obviates the need to do absolute radiometry has been performed, and it is reported in this volume. In that case, the results agree well with the CCV9 results and do not agree with the UDW within the expanded uncertainty. It has been noted already in the Introduction that measurements on other Na-like ions using the MEIBEL technique agree well with the close-coupling theory.

ACKNOWLEDGMENTS

This work was supported in part of the Office of Fusion Energy Sciences of the U.S. Department of Energy through Contract No. DE-A102-95ER54293 with the US National Institute of Standards and Technology. The authors gratefully acknowledge assistance of J. W. Hale in operation of the ORNL-PIG ion source.

APPENDIX: CALIBRATION

To obtain an absolute cross section, it is necessary to determine both $D(z_0,\lambda)$ in Eq. (3) and $D_R(z,\lambda)$ in Eq. (5).

TABLE II. Individual sources of uncertainty in the assessment of radiometric sensitivity; presented at the 1σ level. A coverage factor of 1.7 is used in presenting the total in Table I.

Source of uncertainty in spectroradiometry	% uncertainty, 1σ level
Ignoring decay length	<0.1
Dead time correction	± 1
Interference filter correction for angle of incidence	<0.1
Determination of pulse counting efficiency	± 0.5
Numerical integrations	± 1
Determination of step size	± 1
Measurements of Z_0, diameters of limiting apertures, and other geometric factors	± 1
Calibration of electrometer for diode comparison	± 7.5
NBS (NIST) calibration of photodiodes	± 9
Photodiode to photomultiplier transfer (scattered light, spatial uniformity, etc.)	± 2
Scattered light in crossed beams apparatus	± 2
Quadrature sum	± 9.8
Anistropy of light:	
Threshold	$+0.5$
High energy limit	-1.2

Since the response of a photomultiplier generally varies substantially over its surface, it was necessary to map out the response in detail. Then $D_R(z,\lambda)$ was obtained from

$$D_R(z,\lambda) = \frac{D_B}{4\pi}\int D_r(x',y',\lambda)\frac{\cos(\gamma)}{r^2}T(\gamma)dx'\,dy', \tag{A1}$$

where $D_r(x',y',\lambda)$ is the relative sensitivity at wavelength λ of the photocathode at positions x',y' on its surface, D_B is the sensitivity of the photocathode at some chosen benchmark position such that $D_R(z_0,\lambda)=1$, λ is the angle off of normal for the photon, $T(\lambda)$ is the transmission of the interference filter and windows as a function of λ, and r is the distance from the point of emission to the spot on the photocathode, $r=[(x')^2+(y')^2+z^2]$. The integral is performed over a number of different values of z and fitted to within 0.03% to the functional form $(z^0/z)^2$.

The calibration arrangement is illustrated in Fig. 3. Photons of wavelength 184.95 nm from a Hg discharge lamp were selected with a 3/4 m vacuum monochromator. Light from the monochromator could be transported to two ports using a stationary spherical mirror and a plane mirror which could be rotated about two axes. The motion of the plane mirror allowed the detector sensitivity, including the supersil window, to be mapped out; thus giving $D_r(x',y',\lambda)$. The motion also allowed a calibration transfer from one of two NIST-calibrated photodiodes [39] to the benchmark point on the detector, thus determining $D(z_0,\lambda)$. The variation of the photomultiplier sensitivity over its surface is shown in Fig. 4. The strong variation illustrates the need to have a well-defined reference point as well as the need to carefully integrate over surface. The value of $D(z_0,\lambda)$ was determined both before and after the experimental measurements and the values obtained agreed within 0.3%. A wavelength correction of 1% between 184.95 nm from the Hg lamp used in calibration and the weighted average of the Al^{2+} doublet at 185.74 nm was determined using a quasicontinuous, though less bright discharge lamp.

The supersil window transmission was determined separately and found to agree with the manufacturer's specifications. The window was examined using a polariscope and found to be free of strains that might have been present due to mounting. The amount of scattered light entering the detector was shown in separate tests using an isotropic light source to be $\sim 2\%$ ($\pm 2\%$).

Uncertainties associated with the radiometry are listed in Table II at the 1σ level. Two-sided uncertainties are combined in quadrature, and one-sided uncertainties are added linearly both here and in Table I. A coverage factor of 1.7 to give an equivalent 90% C.L. has been used in entering values from Table II into Table I.

[1] For example, K. Butler, in *Atomic and Molecular Data and Their Applications*, edited by Peter J. Mohr and Wolfgang L. Wiese, AIP Conf. Proc. No. **434** (AIP, New York, 1997), p. 23.

[2] D. R. Flower and N. Nussbaumer, Astron. Astrophys. **42**, 265 (1975); F. P. Keenan, P. L. Dufton, and A. E. Kingston, *ibid.* **169**, 319 (1986).

[3] K. C. Mathur, A. N. Tripathi, and S. K. Joshi, Int. J. Mass Spectrom. Ion Phys. **7**, 167 (1971).

[4] J. Davis and S. Morin, J. Quant. Spectrosc. Radiat. Transf. **11**, 463 (1971); **11**, 495 (1971).

[5] Yong-Ki Kim and Kwok-tsang Chang, Phys. Rev. A **18**, 36 (1978).

[6] A. L. Merts, J. B. Mann, W. D. Robb, and N. H. Magee, Jr., Los Alamos Laboratory Informal Report No. LA-8267-MS, 1980 (unpublished); (private communication).

[7] P. L. Dufton and A. E. Kingston, J. Phys. B **20**, 3899 (1987).

[8] J. Mitroy and D. W. Norcross, Phys. Rev. A **39**, 537 (1989).

[9] For examples see: H.-J. Kunze, Space Sci. Rev. **13**, 565 (1972); A. H. Gabriel and C. Jordan, in *Case Studies in Atomic Collision Physics II*, edited by E. W. McDaniel and M. R. C. McDowell (North-Holland, Amsterdam, 1972), p. 209; B. C. Boland, F. C. Jahold, T. J. L. Jones, and R. W. P. McWhirter, J. Phys. B **3**, 1134 (1970).

[10] For examples see: D. F. Dance, M. F. A. Harrison, and A. C. H. Smith, Proc. R. Soc. London, Ser. A **290**, 74 (1966); F. M. Bacon and J. W. Hooper, Phys. Rev. **178**, 182 (1969).

[11] For examples see: E. K. Wåhlin, J. S. Thompson, G. H. Dunn, R. A. Phaneuf, D. C. Gregory, and A. C. H. Smith, Phys. Rev. Lett. **66**, 157 (1991); E. W. Bell, X. Q. Guo, J. L. Forand, K. Rinn, D. R. Swenson, J. S. Thompson, M. E. Bannister, D. C.

Gregory, R. A. Phaneuf, A. C. H. Smith, A. Müller, C. A. Timmer, E. K. Wåhlin, B. D. DePaola, and D. S. Belić, Phys. Rev. A **49**, 4585 (1994).
[12] For examples see: S. J. Smith, K-F. Man, R. J. Mawhorter, I. D. Williams, and A. Chutjian, Phys. Rev. Lett. **67**, 30 (1991); S. J. Smith, A. Chutjian, J. Mitroy, S. S. Tayal, R. J. W. Henry, K-F. Man, R. J. Mawhorter, and I. D. Williams, Phys. Rev. A **48**, 292 (1993).
[13] For examples see: R. E. Marrs, M. A. Levine, D. A. Knapp, and J. R. Henderson, Phys. Rev. Lett. **60**, 1715 (1988); S. Chantrenne, P. Beiersdorfer, R. Cauble, and M. B. Schneider, *ibid.* **69**, 265 (1992).
[14] For example, R. A. Phaneuf, in *The Physics of Electronic and Atomic Collisions*, edited by Torkild Andersen, Bent Fastrup, Finn Folkmann, Helge Knudsen, and N. Andersen, AIP Conf. Proc. No. **295** (AIP, New York, 1993), p. 405.
[15] P. O. Taylor, D. Gregory, G. H. Dunn, R. A. Phaneuf, and D. H. Crandall, Phys. Rev. Lett. **39**, 1256 (1977).
[16] D. Gregory, G. H. Dunn, R. A. Phaneuf, and D. H. Crandall, Phys. Rev. A **20**, 410 (1979).
[17] D. W. Savin, L. D. Gardner, D. B. Reisenfeld, A. R. Young, and J. L. Kohl, Phys. Rev. A **51**, 2162 (1995).
[18] R. A. Phaneuf, P. O. Taylor, and G. H. Dunn, Phys. Rev. A **14**, 2021 (1976).
[19] D. S. Belić, R. A. Falk, G. H. Dunn, D. Gregory, C. Cisneros, and D. H. Crandall, Bull. Am. Phys. Soc. **26**, 1315 (1981). Brief report at the annual meeting of the APS Division of Electron and Atomic Physics, 1981.
[20] M. E. Bannister, H. Krause, N. Djurić, D. B. Popović, G. H. Dunn, Y.-S. Chung, and A. C. H. Smith, Phys. Rev. A **66**, 032707 (2002).
[21] S. J. Smith, A. Chutjian, J. Mitroy, S. S. Tayal, R. J. W. Henry, K-F. Man, R. J. Mawhorter, and I. D. Williams, Phys. Rev. A **48**, 292 (1993).
[22] E. K. Wåhlin, J. S. Thompson, G. H. Dunn, R. A. Phaneuf, D. C. Gregory, and A. C. H. Smith, Phys. Rev. Lett. **66**, 157 (1991).
[23] N. Djurić, M. E. Bannister, A. M. Derkatch, D. C. Griffin, H. F. Krause, D. B. Popović, A. C. H. Smith, B. Wallbank, and G. H. Dunn, Phys. Rev. A **65**, 052711 (2002).
[24] X. Q. Guo, E. W. Bell, J. S. Thompson, G. H. Dunn, M. E. Bannister, R. A. Phaneuf, and A. C. H. Smith, Phys. Rev. A **47**, R9 (1993).
[25] P. O. Taylor and G. H. Dunn, Phys. Rev. A **8**, 2304 (1973).
[26] W. T. Rogers, J. O. Olsen, and G. H. Dunn, Phys. Rev. A **18**, 1353 (1978).
[27] M. L. Mallory and D. H. Crandall, IEEE Trans. Nucl. Sci. **23**, 1069 (1976).
[28] F. M. Bacon and J. W. Hooper, Phys. Rev. **178**, 182 (1969).
[29] Derivation of the equations here can be found in P. O. Taylor, Ph.D. thesis, University of Colorado, 1972, available through University Microfilms International, Dissertation Copies, P.O. Box 1764, Ann Arbor, MI 48106. Order no. 73-18,602.
[30] D. H. Crandall, R. A. Phaneuf, and P. O. Taylor, Phys. Rev. A **18**, 1911 (1978).
[31] P. O. Taylor, K. T. Dolder, W. E. Kauppila, and G. H. Dunn, Rev. Sci. Instrum. **45**, 538 (1974).
[32] H. S. W. Massey and E. H. S. Burhop, *Electronic and Ionic Impact Phenomena* (Oxford, Clarendon, 1969), Vol. I, p. 656.
[33] Acton Research, Model 185-N. Peak wavelength 183.0 nm, bandwidth 25.5 nm, peak transmission 29%, transmission at 186 nm is 27%.
[34] Hamamatsu type 1460; Cs-Te cathode.
[35] I. C. Percival and M. J. Seaton, Philos. Trans. R. Soc. London **251**, 113 (1958).
[36] J. V. Kennedy, V. P. Myerscough, and M. R. C. McDowell, J. Phys. B **11**, 1303 (1977).
[37] U. Fano and J. H. Macek, Rev. Mod. Phys. **45**, 553 (1973).
[38] G. H. Dunn, in *Atomic Physics*, edited by B. Bederson, V. W. Cohen, and F. M. J. Pichanick (Plenum, New York, 1969), p. 417.
[39] The ''primary'' diode, SEL No. 152, was calibrated by NBS (now NIST) just six months prior to use with a quoted probable error of 6%. The second diode, EMR model 543P-09-00 was calibrated by NBS two years prior to use with a quoted probable error of 6%. Comparison of the two diodes showed agreement within 3%.